THE ASTROPHYSICAL JOURNAL, 418:100–112, 1993 November 20

HIGH-RESOLUTION CO AND H I OBSERVATIONS OF THE INTERACTING GALAXY NGC 3627

XIAOLEI ZHANG,[1,2] MELVYN WRIGHT,[1] AND PAUL ALEXANDER[3]
Received 1993 February 12; accepted 1993 April 28

ABSTRACT

A nearby normal spiral galaxy, NGC 3627, which is a member of the interacting group the Leo Triplet, is mapped in the CO 1–0 transition for its central 4.5 kpc region using the Berkeley-Illinois-Maryland Association (BIMA) interferometer array with 7″ resolution, and in the 21 cm emission of neutral hydrogen for the entire galaxy using the Very Large Array (VLA) with 30″ resolution. The combined CO and H I data provide new information, both on the history of the past encounter of NGC 3627 with its companion galaxy NGC 3628 and on the subsequent dynamical evolution of NGC 3627 as a result of this tidal interaction. In particular, the morphological and kinematic information indicates that the gravitational torque experienced by NGC 3627 during the close encounter triggered a sequence of dynamical processes, including the formation of prominent spiral structures, the central concentration of both the stellar and gas mass, the formation of two widely separated and outwardly located inner Lindblad resonances, and the formation of a gaseous bar inside the inner resonance. These processes in coordination allow the continuous and efficient radial mass accretion across the entire galactic disk. The observational result in the current work provides a detailed picture of a nearby interacting galaxy which is very likely in the process of evolving into a nuclear active galaxy. It also suggests one of the possible mechanisms for the formation of successive instabilities in postinteraction galaxies, which could very efficiently channel the interstellar medium into the center of the galaxy to fuel nuclear starburst and Seyfert activities.

Subject headings: galaxies: evolution — galaxies: individual (NGC 3627) — galaxies: interactions — galaxies: ISM — galaxies: structure

1. INTRODUCTION

In recent years it has become increasingly apparent that the interaction among galaxies plays an important role in the evolution of a disk galaxy. Statistical study of the distribution of interacting galaxies at different redshifts indicates that most galaxies have suffered various degrees of gravitational interactions with neighboring galaxies in their lifetime (Zepf & Koo 1989; Efstathiou 1990; Barnes & Hernquist 1992). It is also found that nuclear activity and starburst phenomena observed in many galaxies seem to correlate with these galaxies being in compact groups or clusters, or else have companion galaxies (see, for example, Adams 1977; Simkin, Su, & Schwarz 1980; Stockton 1982; Hutchings & Campbell 1983; Dahari 1985; see also the many contributions included in Wielen 1990 and Sulentic, Keel, & Telesco 1990).

The effect of galaxy interaction on the galactic mass distribution was first investigated by Toomre & Toomre (1972) using restricted three-body calculations. Their models showed furious response of the disk mass for prograde encounters in the form of bridges, tails, and spiral patterns. Retrograde encounters showed much weaker response, which is partly physical and also partly because self-gravity of the particles constituting the disk was not taken into account in these kinematic models. In recent years several theoretical and numerical studies have been carried out to investigate the effect of tidal interactions on the excitation of disk instabilities, and on the removal of angular momentum from the interstellar medium, so as to channel the gas to the center of a galaxy to fuel nuclear activity. Byrd et al. (1986) studied the effect of the gravitational tide produced by companion galaxies in triggering large-scale gravitational instabilities in the galactic disk. They found that the tidal interactions decreased the disk instability threshold, and the required level of tidal perturbation for inducing significant nuclear inflow matched the strength of the observed galaxy interactions. Lin, Pringle, & Rees (1988) supplemented the analysis of Byrd by proposing that the propagation of the effect of tidal perturbation to the inner disk is enhanced if the "swing-amplification" mechanism for the global spiral pattern is taken into account. The above mechanisms could account for the removal of angular momentum and the radial accretion of mass down to the central 1–2 kpc radius, where the large-scale spiral structure weakens. In the same paper, Lin et al. (1988) also proposed a mechanism for the continuous central channeling of gas, needed to bridge the gap between the radius of ~ 1 kpc, where the swing amplifier runs out of steam, and the radius of 0.1–1 pc, where the accretion disk around the central black hole takes over. Lin et al. (1988) proposed that the gas in the inner kiloparsec of a galaxy is in nearly circular motion in a gaseous disk. The effect of the galactic interaction propagates inward and perturbs the cloud orbits. This results in increased cloud-cloud collision and the subsequent rapid cooling of the gas material. The increase in the importance of gas self-gravity as a result of cooling leads to an increase in gas viscosity and an enhanced mass accretion rate. Another model by Shlosman, Frank, & Begelman (1989) proposed a so-called bars-within-bars scenario. In this model, within the background of a large-scale stellar bar, a central gaseous bar forms as a result of the gravitational instability, induced by the increased mass accretion from the outer disk onto the central self-gravitating gaseous disk. This process of the formation of

[1] Radio Astronomy Laboratory, University of California at Berkeley, Berkeley, CA 94720.
[2] Harvard-Smithsonian Center for Astrophysics, 60 Garden Street, Cambridge, MA 02138.
[3] Mullard Radio Astronomy Observatory, Cavendish Laboratory, Madingley Road, Cambridge, CB3 0HE, England.

successive gravitational instabilities at different radii provides a possible mechanism for the continuous central channeling of gas across the galactic disk.

Since few interacting galaxies have been mapped with high resolution to confine theoretical models, a detailed picture of the type of instabilities that occur and the nature of the mass accretion process in the inner kiloparsec region of a spiral galaxy is still lacking. Other related questions, such as the role of the underlying stellar disk, especially the influence of the redistribution of stellar mass to the postencounter evolution of gaseous distribution, and to the evolution of normal to active galaxies, are hardly even addressed.

In order to look into the various unanswered questions in the galactic interaction and evolution process, and especially in order to obtain detailed information for the central region of a postinteraction galaxy, where the global spiral pattern and the nuclear instability structure meet, we have mapped a nearby interacting spiral galaxy NGC 3627 in the CO 1–0 transition and in the 21 cm emission of neutral hydrogen (H I), using the aperture synthesis technique. The CO 1–0 observations were made with the Berkeley-Illinois-Maryland Association (BIMA) millimeter interferometer to obtain a 7″ resolution image for the central 4.5 kpc region. The H I observations were made using the Very Large Array (VLA) with 30″ resolution, and cover the entire optical galaxy disk.

NGC 3627 is a member of an interacting group, the Leo Triplet, whose other two members are NGC 3628 and NGC 3623. It is relatively nearby, at a distance of 6.7 Mpc according to de Vaucouleurs (1975). It has an inclination angle of about 60°, which allows its velocity field to be obtained and at the same time the components which generate these velocities to be identified. The single-dish data for CO 1–0 (Young, Tacconi, & Scoville 1983) and H I (Haynes, Giovanelli, & Morton 1979), as well as the optical image, are all available for comparison. Numerical modeling of the encounter process between NGC 3627 and NGC 3628 had also been carried out (Toomre 1977; Rots 1978).

Although classified as a normal spiral [RC2 type SAB(s)b], NGC 3627 has certain unusual properties, such as a high H_2 to H I mass ratio, close to that appropriate for Seyfert galaxies (Young et al. 1983), and a reasonably strong nuclear Hα emission line indicating that it is currently undergoing at least a weak form of nuclear starburst (Filippenko & Sargent 1985). It also has a weak optical bar, two prominent spiral arms, and prominent dust lanes (Arp 1966). These characteristics indicate that NGC 3627 is possibly a borderline galaxy, with properties between those of normal and active galaxies, and thus is an ideal candidate for studying the postinteraction evolution and the process of the transition from normal galaxies to nuclear active galaxies as a result of interaction-triggered instabilities.

2. PREVIOUS OBSERVATIONS AND SIMULATIONS OF THE LEO TRIPLET

NGC 3627, NGC 3628, and NGC 3623 form the well-known interacting group, the Leo Triplet. The past encounters between NGC 3627 and NGC 3628 left traces of distortion in both galaxies. The most noticeable one is a plume in the galaxy NGC 3628 which shows up both in the optical (Zwicky 1956; Kormendy & Bahcall 1974) and in H I (Rots 1978; Haynes et al. 1979), emerging from the eastern tip and extending about 50′ from the center of the galaxy. Recent observations also indicate the presence of a 100 μm plume (Appleton & Hughes 1988). The emission profiles observed along the plume of NGC 3628 show substructure with velocity width less than 17 km s^{-1} over scales of 6.4 kpc and an almost constant velocity over more than 50 kpc in length. This is the narrowest known extragalactic neutral hydrogen emission profile. Distortions in NGC 3627 have also been found, including large-scale asymmetry and a counterrotating H I envelope near the southeast part of the galactic disk. A reproduction of the H I observations of the Leo Triplet by Haynes et al. (1979) overlaid on the optical image is given in Figure 1, showing the relative positions of these three galaxies and their large-scale morphology.

Young et al. (1983) observed the Leo Triplet galaxies in the CO 1–0 transition using the FCRAO 14 m (HPBW = 50″) telescope. In both NGC 3627 and NGC 3628 the CO emission peaks toward the nucleus, with less emission at larger radii along the major axis. No CO emission was detected from NGC 3623 or the plume.

The molecular mass inferred in the observations of Young et al. (1983), using a standard CO flux and H_2 mass conversion ratio, is $\gtrsim 10^9$ $M_\odot$ for both NGC 3627 and NGC 3628. But the H I mass derived by Haynes et al. (1979) for NGC 3627 is a factor of 10 lower than that for NGC 3628. The total $M(H_2)/M(H\ I)$ ratio is 3.7 for NGC 3627, similar to that observed in the Seyfert galaxy NGC 1068 (Scoville & Young 1983). This situation is unique among normal Sb and Sc galaxies (Young & Scoville 1982a, b). Young et al. (1983) attribute this high $M(H_2)/M(H\ I)$ ratio in NGC 3627 to an enhanced conversion of H I to H_2 as a result of the interaction with NGC 3628. Our observational data later show that, at least for the outer disk region of NGC 3627, another plausible cause is that of NGC 3627 lost part of its H I outer envelope during the encounter with NGC 3628. Young et al. (1983) also found that the ratio of the blue to CO luminosities in the central 5 kpc for both NGC 3627 and NGC 3628 is similar to the ratio measured previously by Young & Scoville (1982b) for field Sc galaxies and Sc galaxies in the Virgo Cluster. If this ratio is interpreted as an indicator of the efficiency of star formation per unit H_2 mass, then the tidal interaction of these galaxies has not greatly changed the star formation efficiency. If the tidal encounter between NGC 3627 and NGC 3628 triggered the formation of molecular clouds in the galactic disk, these clouds have already formed stars and are now beyond the initial burst stage.

Toomre (1977) and Rots (1978) have separately modeled the encounter of NGC 3627 with NGC 3628 using similar model parameters, treating it as a restricted three-body problem. In their models, NGC 3627, modeled as a point mass, passed NGC 3628 in a parabolic orbit, and the orbit of the encounter is in the direct sense of galactic rotation for NGC 3628 (but in the retrograde sense for NGC 3627 in reality). Figure 2 is a reproduction of Rot's (1978) simulation results. This kinematic model accurately reproduced the current morphology of NGC 3628 in both the spatial and the velocity space. For the best-fit model parameters, the perigalacticon happened 8×10^8 years ago, and the perigalacticon distance is about 25 kpc.

Although experiencing a retrograde encounter, previous observations have shown that NGC 3627 also displayed signs of distortion as a result of the interaction, such as the optical "hook" extending far to the northwest of this galaxy (Arp 1966) and the distorted neutral hydrogen distribution in the outer disk of NGC 3627 (Haynes et al. 1979). The H I velocity in the southeastern part of the envelope is almost in the opposite sense of the galactic rotation for that region. Never-

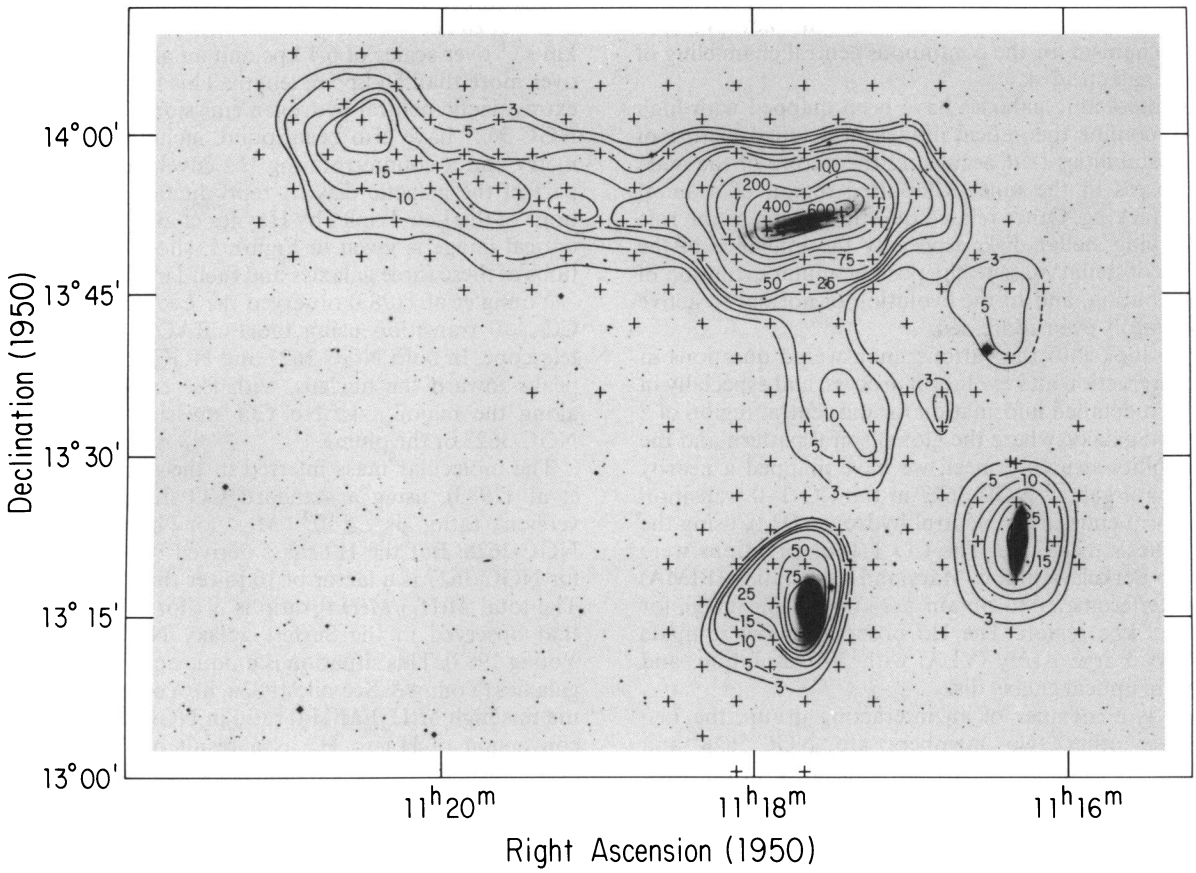

FIG. 1.—Reproduction of H I observations of the Leo Triplet by Haynes et al. (1979), using the Arecibo telescope with angular resolution of 3.3, overlaid on the optical image from the Palomar Sky Survey print.

theless, NGC 3627 shows a lesser degree of damage compared with NGC 3628. This is mainly because, as Toomre (1977) pointed out, the orbit of encounter for NGC 3627 is almost retrograde with respect to the rotation of this galaxy (the eastern side is near, the southern side is receding), while for NGC 3628 the encounter is in the prograde sense. Retrograde encounters usually cause less distortion to galaxy mass distribution than direct encounters (e.g., Toomre & Toomre 1972).

A summary of the basic parameters of NGC 3627 is given in Table 1.

3. CO 1–0 AND H I APERTURE SYNTHESIS OBSERVATIONS OF NGC 3627

3.1. *CO Observations*

The CO 1–0 aperture synthesis observations of the galaxy NGC 3627 were obtained between the spring of 1990 and the spring of 1992, using the BIMA array. The cooled Schottky diode receiver gave an average system temperature of about 1000 K at 115 GHz. The 512 channel digital correlator provided a velocity coverage of 832 km s^{-1} and a velocity resolution of 3.25 km s^{-1} per channel. The FWHM of the main beam at this frequency is a little less than 2′. The galaxy was observed using both the C-array configuration, which gives an angular resolution of 15″, and the B-array configuration, which gives an angular resolution of 7″. The data from both array configurations were combined to obtain a high-resolution image without losing significant flux. The best signal-to-noise ratio is obtained with natural weighting of the visibility data, yielding a synthesized beam size of 9″ × 12″.

The amplitude and phase of the visibility data, as well as the instrumental passband, were all calibrated by observing the bright quasar 3C 273, which is located close to the source. Planets were usually observed at the beginning or the end of each configuration to check flux calibration. The flux scale was set according to Ulich's (1981) measurement for planets. The flux calibration is believed to be accurate to within 20%.

The calibration and analysis of the data were made using the software packages RALINT and MIRIAD, developed at BIMA. Maps were made by averaging 10–15 channels of visi-

TABLE 1

GALAXY PARAMETERS

Parameter	Value
R.A. (1950)[a]	$11^h17^m37^s.9$
Decl. (1950)[a]	13°16′08″
RC2 type[b]	SAB(s)b
Inclination[b]	60°
Position angle[b]	173°
V_{LSR}[c]	700 km s^{-1}
Distance[b]	6.7 Mpc
Angular scale corresponding to 1 kpc[b]	31″

[a] Dressel & Condon 1976.
[b] de Vaucouleurs, de Vaucouleurs, & Corwin 1976 (RC2).
[c] Young, Tacconi, & Scoville 1983.

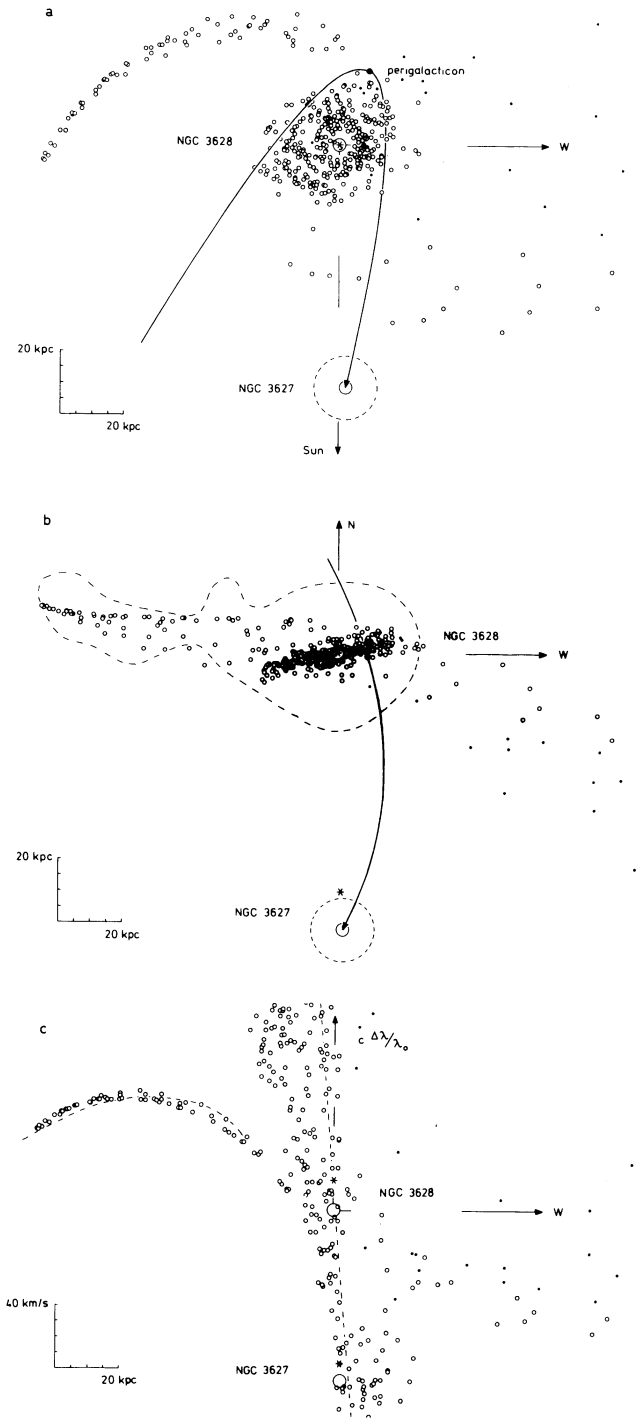

FIG. 2.—Reproduction of the kinematic model of Rots (1978) for the encounter of NGC 3627 with NGC 3628. (*a*) View from the north direction. (*b*) Projection onto the plane of the sky. (*c*) Projection onto the (right ascension, Doppler velocity)-plane.

bility data to enhance the signal-to-noise ratio. The maps were deconvolved using the CLEAN algorithm to remove the synthesized beam sidelobes.

An integrated intensity map (moment 0) for the velocity range of 400–900 km s^{-1} is shown in Figure 3. The synthesized beam size is about 9″ × 12″, with its major axis in the north-south direction. Primary-beam correction was not made. Each

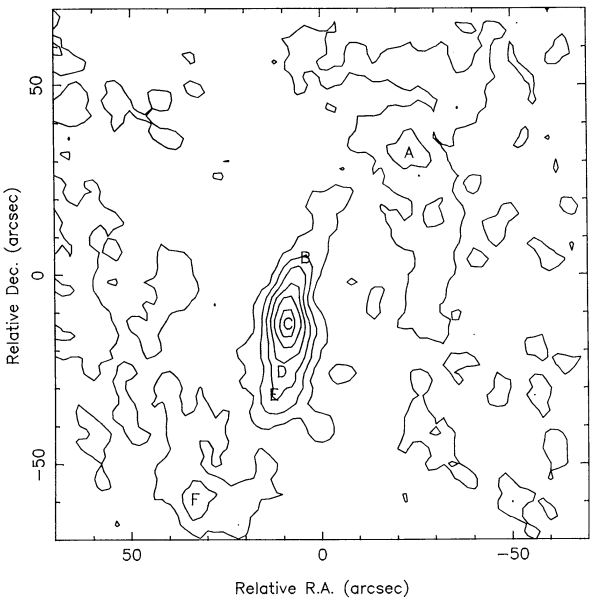

FIG. 3.—Integrated intensity map from the CO 1–0 aperture synthesis observations. The contour levels are 0.04 (σ), 0.07, 0.11, 0.15, 0.18, and 0.22 K, respectively, with a velocity width of 550 km s^{-1}. The letters on the map are used to indicate positions where the spectra will be shown later.

of the 50 km s^{-1} velocity-channel maps were clipped at 0.4 times the original channel noise level before adding the maps. This operation improved the map quality, and no noticeable difference in the map maximum was found between the clipped and unclipped integrated maps. The 50 km s^{-1} is close to the velocity width of CO emission within the current synthesized beam size; thus this choice of the channel width optimized the signal-to-noise ratio in the channel maps.

The map center we used for the CO (and also H I) aperture synthesis observations, R.A. = 11^{h}17^{m}37^s.9 and decl. = 13°16′8″, is not the true dynamical center of the galaxy, which is offset in (x,y) directions by (−8″.8, −12″.2), as this CO high-resolution map reveals. The CO distribution near the center of the galaxy is in the form of an asymmetric barlike structure, located to the southeast of the map center. A short distance away from the end of the molecular bar, we can see the beginning of the spiral arms.

Figure 4 shows the velocity-channel maps of CO observations for every 100 km s^{-1}. The numbers marked in the right-hand corners of each map indicate the central velocities of each channel. For the central 300 km s^{-1} range (550–650, 650–750, and 750–850 km s^{-1}), a clear rotation trend can be seen.

3.2. H I *Observations*

The H I observations of NGC 3627 were obtained with the VLA in C- and D-array configurations during 1988. We used the same central position as in our CO aperture synthesis observations, and as used in the previous single-dish observations in H I by Haynes et al. (1979) and in CO by Young et al. (1983). The angular resolution is about 30″. The integration time on source was approximately 2.5 hr in C-array and 1.5 hr in D-array. All observations were made in observing mode 1A/1C at a heliocentric velocity of 790 km s^{-1} with on-line Hanning smoothing applied. With a total of 63 channels we obtained a velocity resolution of 20.6 km s^{-1} and a total bandwidth of 6.25 MHz (1320 km s^{-1}). The flux calibrator was 3C 286, and 1117+146 was used as a phase calibrator which was

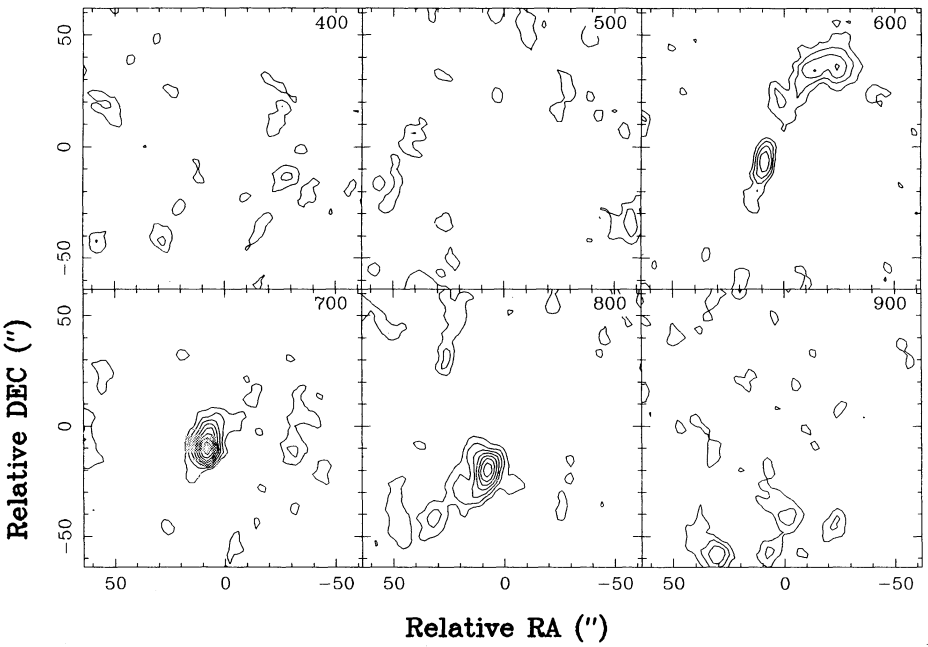

FIG. 4.—Velocity-channel maps of CO 1–0 aperture synthesis observations

observed at least every 30 minutes. The integration time was 60 s. The data editing and calibration were done using the AIPS package, and the continuum was removed by subtracting the average of line-free channels from all channels. The observed baselines were flat, and no additional correction was applied. For quantitative analysis a spectral line data cube was produced and CLEANed. The calibrated data were then converted from the FITS format to the MIRIAD format and were analyzed together with the CO data.

Figure 5 shows the moment 0 map of H I from 450 to 1050 km s^{-1}, with about 30″ resolution. A 1.5 σ (here σ is the noise level in the channel maps) noise clipping in each of the 20 km s^{-1} velocity-channel maps was made before summation. This clipping operation was found to alter the map maximum by about 10%. Primary-beam correction was not made. Figure 5 displayed the distortion and asymmetry of the H I spiral arms, especially in the southeast part of the galaxy where a separate piece of material (indicated by the letter L) is resolved, which coincides with the region of the counterrotating envelope observed by Haynes et al. (1979) at lower resolution.

Figure 6 shows the H I velocity-channel maps for every 50 km s^{-1}. The gradual emergence and disappearance of the different parts of the two spiral arms as we advance in velocity are a manifestation of the galactic rotation. A notable feature here is the southeastern clump in the velocity windows of 850–900 km s^{-1} and 900–950 km s^{-1}, at the same spatial location as the resolved feature L in the integrated intensity map. The clump apparently does not follow the galactic rotation, and its characteristics and origin will be discussed more fully later.

Figure 7 shows an overlay of the CO and H I integrated intensities for NGC 3627. Note that the H I image covers the entire optical galaxy, whereas the CO observations cover only the central 140″ × 140″. The CO barlike feature is seen to reside inside the central H I deficiency. Two CO clumps farther out coincide with the H I clumps at the same locations, which trace the beginning of the spiral arms. The H I and CO distributions show evidence of asymmetry and distortions. The

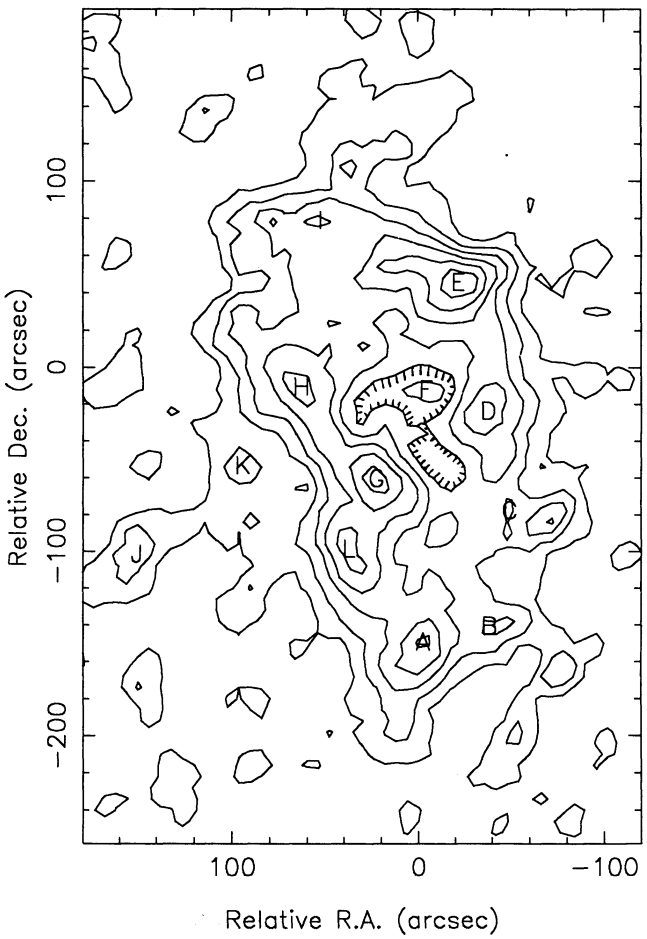

FIG. 5.—Integrated intensity map from H I aperture synthesis observations. The contour levels are 0.06, 0.12 (σ), 0.18, 0.25, 0.31, and 0.37 K, respectively, with a velocity width of 620 km s^{-1}. The letters on the map are used to indicate positions where the spectra will be shown later.

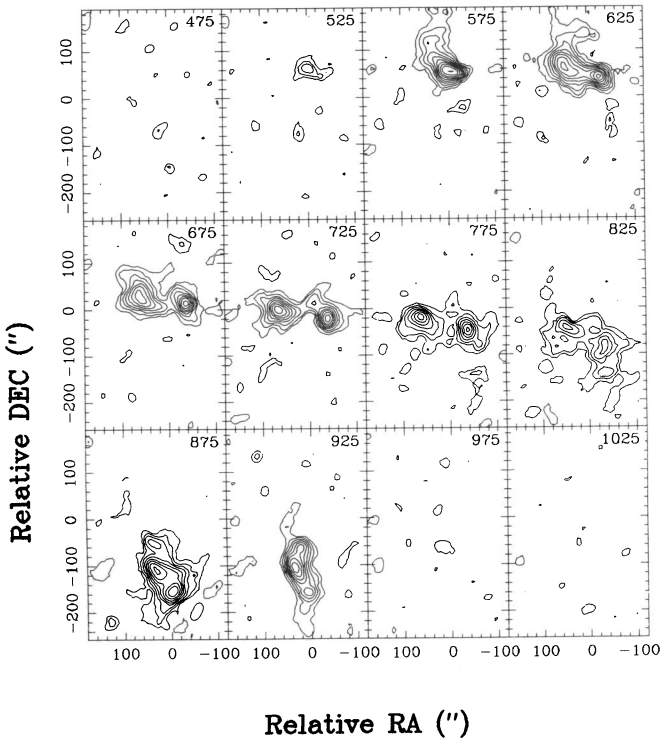

FIG. 6.—Velocity-channel maps of H I aperture synthesis observations

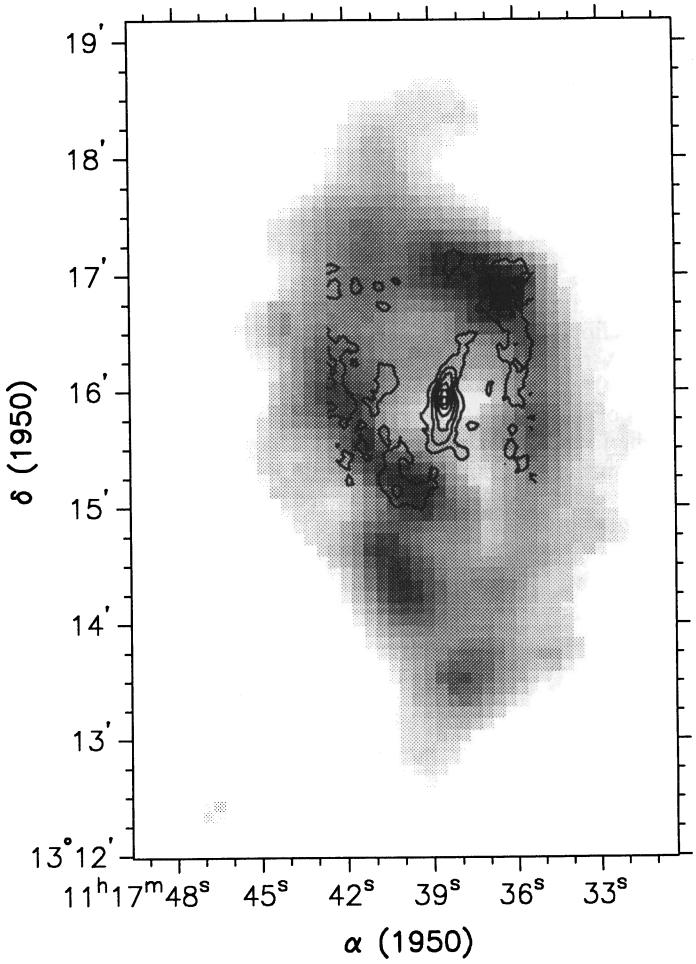

FIG. 7.—Overlay of the CO (*contours*) and H I (*halftone*) aperture synthesis images. The CO observation covers only the central 140″ × 140″.

morphological characteristics and their implication for the dynamics of NGC 3627 will be discussed in more detail in § 4.

4. ANALYSIS AND DISCUSSION

In what follows, the combined CO and H I aperture synthesis data will be used to study the mass content and kinematics of the galaxy, and to infer the dynamical process which gives rise to the present galactic conditions.

4.1. *Estimation of the ISM and Dynamical Mass*

4.1.1. *Radial Distribution of the Column Densities of the Molecular and Atomic Gas*

The optically thin H I column density is estimated using the relation

$$N_{\rm H\,I}({\rm cm}^{-2}) = 1.823 \times 10^{18} \int_V T_B^{\rm H\,I}\, dV({\rm K\ km\ s}^{-1})\,, \quad (1)$$

and the H_2 column density is estimated using the empirical relation (Young & Scoville 1982a)

$$N_{\rm H_2}({\rm cm}^{-2}) = 4.1 \times 10^{20} \int_V T_B^{\rm CO}\, dv({\rm K\ km\ s}^{-1})\,, \quad (2)$$

where the numerical coefficient chosen is consistent with the value used in Young et al. (1983). Here the choice of using the empirical formula for the conversion of CO luminosity to H_2 column density is partly justified from the estimation of the excitation temperature using the CO 2–1 and CO 3–2 data obtained at CSO (Zhang 1992). A calculated excitation temperature of 20 K confirms that NGC 3627 is not currently undergoing violent starburst; the empirical formula derived from Galactic observations and commonly used for normal galaxies should be a good approximation for this galaxy.

The derived H_2 and H I surface density distributions averaged in elliptical annular rings around the (corrected) center of the galaxy are given in Figure 8. The surface density of H_2 is seen to dominate H I in the center of the galaxy by two orders of magnitude.

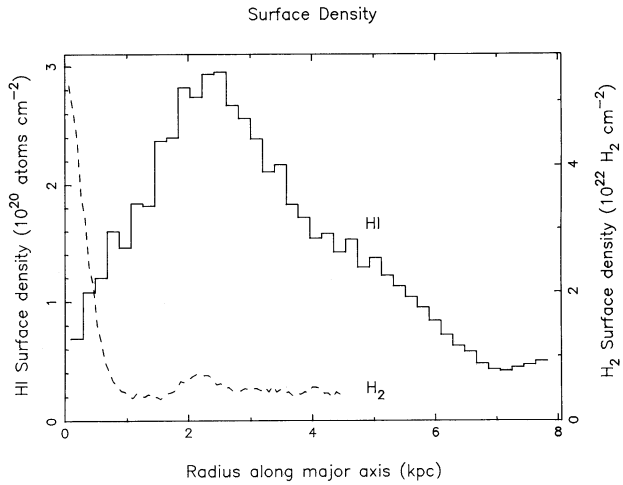

FIG. 8.—H I and H_2 surface density distributions averaged on annular rings around the galactic center.

4.1.2. *Estimation of the ISM Mass*

The total H I mass in the galaxy can be estimated by integrating the H I column density, or equivalently by using the formula

$$M_{\rm H\,I}(M_\odot) = 2.36 \times 10^5 D^2({\rm Mpc}^2) \int_V \int_S F_{\rm H\,I}\, d\Omega\, dV({\rm Jy\ km\ s^{-1}}) \tag{3}$$

where F is the flux density and the integrations are over the plane of the galaxy and the observed velocity range. For 1 σ noise clipping in each of the 20 km s^{-1} channel maps and a velocity range from 300 to 1100 km s^{-1}, a total H I mass of $1.2 \times 10^8\ M_\odot$ ($\pm 30\%$) is obtained, compared to the single-dish result of $4.1 \times 10^8\ M_\odot$ (Haynes et al. 1979).

The total molecular mass in the galaxy has been estimated by Young et al. (1983) to be $1.5 \times 10^9\ M_\odot$.

The molecular bar mass detected by the interferometer is estimated using

$$M_{\rm H_2}(M_\odot) = 1.56 \times 10^4 D^2({\rm Mpc}^2) \int_V \int_S F_{\rm CO}\, d\Omega\, dV({\rm Jy\ km\ s^{-1}})\ . \tag{4}$$

This gives $M_{\rm H_2\ bar} = 4 \times 10^8\ M_\odot$ for the unresolved molecular bar mass in the velocity range 400–900 km s^{-1}.

By convolving the interferometer CO spectrum to that obtained by an equivalent 50″ beam at the galactic center, and comparing it with the single-dish CO spectrum of Young et al. (1983), we found that the interferometer data contain about 50% of the single-dish flux at the center of the galaxy.

4.1.3. *Dynamical Mass Determination*

The dynamical mass of a galaxy within radius R can be estimated as

$$M(R) = \left[\frac{V(R)}{\sin\theta_i}\right]^2 R\ , \tag{5}$$

where θ_i is the inclination angle and $V(R)$ is the galactic rotation velocity projected to the line of sight.

For NGC 3627, with an inclination angle of 60°, we obtain

$$M(R)(M_\odot) = 330.9 V^2[({\rm km\ s^{-1}})^2]R({\rm pc})\ . \tag{6}$$

At a distance of 6.7 Mpc, 1 kpc in the plane of the galaxy corresponds to 31″. For the inner 23″ or 750 pc, which corresponds to the major part of the molecular bar, the galactic rotation velocity projected in the line-of-sight direction at the corresponding position is about 100 km s^{-1} (see § 4.3.2).

Therefore, we have

$$M(R = 750\ {\rm pc}) = 2.5 \times 10^9\ M_\odot\ . \tag{7}$$

Compared with the molecular bar mass detected by the interferometer of $4 \times 10^8\ M_\odot$, and taking into account the missing flux (which is about one-half at the position of the molecular bar) due to the interferometer observations, the interstellar medium constitutes a little more than 30% of the galactic dynamical mass near the center of the galaxy.

The dynamical mass for the entire galaxy can be similarly estimated (up to the radius of corotation, which is about 7 kpc [see § 4.2.3 below for the determination of the corotation radius], and using the projected circular velocity at the corotation radius of about 150 km s^{-1}):

$$M(R = 7\ {\rm kpc}) = (330.9)(150^2)(7 \times 10^3) \approx 5.2 \times 10^{10}\ M_\odot\ . \tag{8}$$

This is to be compared with the total interstellar medium mass of $M_{\rm H\,I} + H_{\rm H_2} = 4.1 \times 10^8\ M_\odot + 1.5 \times 10^9\ M_\odot \approx 1.9 \times 10^9\ M_\odot$. Thus the ISM mass constitutes less than 3% of the galaxy dynamical mass up to the radius of corotation.

4.2. *Morphology and Kinematics of the Galaxy*

4.2.1. *General Morphology of the Gas Distribution*

From the overlay map of CO and H I (Fig. 7), we note that the gas distribution has large-scale asymmetry both in the central region and at the outer envelope, with signs of distortion especially near the southeastern part of the galaxy. The distribution of H_2 (inferred from the CO distribution) and H I also display the characteristic "twin peaks" near the beginning of the spiral arms, suggesting that this is near the radius of an inner Lindblad resonance (ILR) where the crowding of the gas streamlines causes the accumulation of the gas mass, similar in certain ways to those discussed by Kenney et al. (1992) for a sample of four galaxies, where the "twin peaks" were located much closer to the nuclear region. The locations of these ILRs have significant implications for the dynamical evolution history of NGC 3627, and these will be discussed further in § 4.3. At a radius of 2 kpc (or 1′), there is a deficiency of H I. A barlike molecular concentration is located in the innermost 1 kpc.

4.2.2. *Central Molecular Bar*

Figure 9 is the integrated intensity map (made with 0.8 σ noise clipping on the individual channel maps) of CO in the velocity range of 500–800 km s^{-1}, highlighting the morphology of the central molecular clump, showing clearly that the major axis of the galaxy (*a*) and the major axis of the molecular bar (*b*) are offset. The apparent bar axis ratio is 3, compared

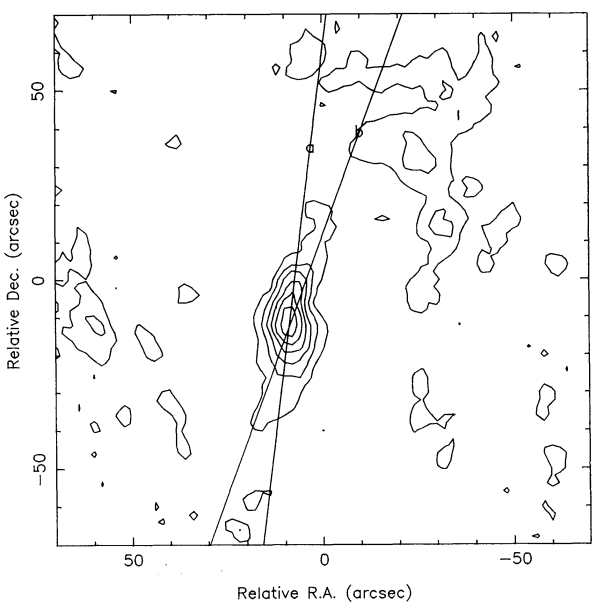

FIG. 9.—Major axes of the galaxy and the molecular bar on a map of velocity range 500–800 km s^{-1}. Channel maps of 50 km s^{-1} have been clipped at the 0.8 σ level before obtaining the integrated map.

with a ratio of 2 expected from a circularly symmetric structure at an inclination angle of 60°. This shows that there is at least some degree of asymmetry in the central molecular mass distribution, although not in the form of a strong bar. The morphology of this barlike structure also indicates a degree of skewness, or the presence of two linear offset mass distributions toward the leading edge of the bar. The CO isovelocity contour map is shown in Figure 10, on which "kinks" on the contours near the two edges of the bar can be observed. These "kinks" coincide in position with the two edges of the skewed mass distribution shown in Figure 9. The morphological and kinematic appearances of the central structure as shown in Figures 9 and 10 suggest that there exist two linear offset shocks at the leading edge of the bar, which is common for a gaseous bar near the galactic center (Roberts, Huntley, & van Albada 1979). This, from another point of view, also confirms the speculation that the central molecular structure is in the form of a molecular bar.

4.2.3. *Rotation Curve and the ILRs*

In order to study in more detail the kinematics and dynamics of the galaxy, we used the combined CO and H I position-velocity maps along the major axis of the galaxy to derive a rotation curve. Following the method of Warner, Wright, & Baldwin (1973), we also made a global fit to the isovelocity contours of H I to derive the rotation curve. Because of the lack of H I near the central region of the galaxy, and the presence of the spiral arm velocity field, the global fit was less successful than using the combined CO and H I position-velocity maps along the major axis. It is also worth mentioning here that, since the CO distribution in the central region of the galaxy is in the form of a weak bar, the gas kinematics is expected to still trace the rotational dynamics of the galaxy.

Figure 11 shows the composite position-velocity map along the major axis of the galaxy, together with a fitted rotation curve. We observe that the rotation curve is asymmetric between the southern and northern part of the galaxy, as had been found before by Young et al. (1983). Since the southern part of the major axis (top part of the rotation curve on this plot, for a position angle of 173°) cuts through the larger portion of the galaxy, we will use the southern rotation curve in most of the following discussion.

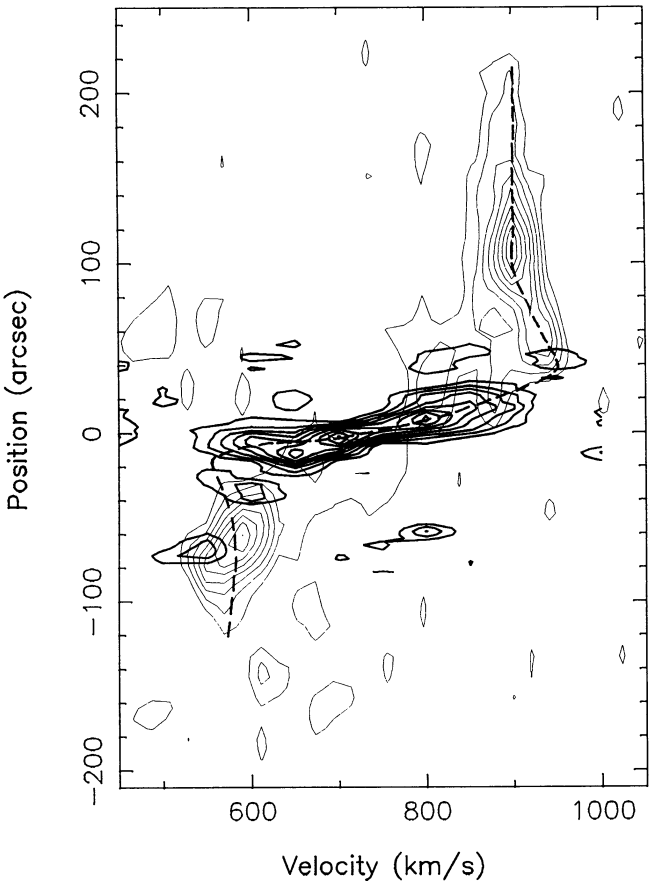

FIG. 11.—Position-velocity map derived from the CO (*dark contours*) and the H I (*lighter contours*) data along the major axis of the galaxy. The dashed line shows the fitted rotation curve.

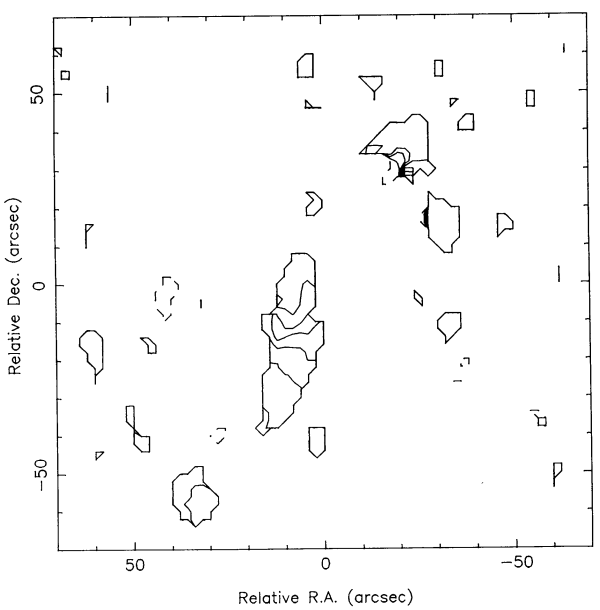

FIG. 10.—Isovelocity contours for the CO bar. Contour levels are 500, 540, 580, 620, 660, 700, 740, 780, and 820 km s^{-1}. Three sigma noise clipping was applied to the channel maps before the moment was taken.

Comparing the rotation curve with the one obtained using the combined CO and H I single-dish data for the same region (Fig. 5 in Young et al. 1983), the high-resolution data now indicate a much steeper rise near the center of the galaxy, and the rotation curve turnover radius is also more accurately determined. Note that the derived rotation curve is not corrected for inclination; in order to obtain the true circular velocity, the projected velocity at each radius should be divided by sin θ_i, where θ_i is the inclination angle of the galaxy. In the following discussions, all the velocities and angular velocities refer to the projected velocities in the plane of the sky.

Using the derived rotation curve, we can further calculate the angular speed, the pattern speed, and the location of the ILRs. The angular speed Ω is determined at each radius through

$$\Omega(R) = \frac{V(R)}{R}, \tag{9}$$

where $V(R)$ is the circular speed at that location.

The pattern angular speed Ω_p is the same as the circular speed at the radius of corotation of the orbiting stars and spiral

pattern. The corotation radius in this case is determined as the radius where the optical spiral arm terminates, or a little farther out (Rohlfs 1977; Kenney et al. 1992), which is about 7 kpc for this galaxy.[4] The locations of the ILRs are defined as the positions where the $\Omega = \Omega_p$ line intersects the $\Omega(R) - \kappa(R)/2$ curve, where κ is the epicyclic frequency and is related to the galactic rotation parameters through

$$\kappa = \left[2 \frac{V}{R} \left(\frac{V}{R} + \frac{dV}{dR} \right) \right]^{1/2} . \quad (10)$$

The derived rotation characteristics for the southern part of the galaxy are shown in Figure 12. Note that the density of the error bars does not indicate the density of data points observed. These are merely the arbitrary locations where the angular velocity and their derivatives are calculated. Also note that since there is a short piece of linear or solid-body rotation curve near the center of the galaxy, as seen in Figure 11, the $\Omega(R)$ curve at the center of the galaxy is expected to have zero derivative. This is not represented very well here due to the sparse data points we chose to calculate velocities and their derivatives. Again the inclination angle correction is not made; thus the true angular velocities can be obtained from the angular velocities drawn here by dividing by sin θ_i. The locations of the ILRs will not be influenced by this rescaling of velocities. We see that there are two intersections of the $\Omega = \Omega_p$ line with the Ω-$\kappa/2$ curve. These are designated the inner-inner Lindblad resonance (IILR), which is the one closer to the galactic center and the outer-inner Lindblad resonance (OILR).

Comparing with the CO–H I overlay map of Figure 7, we see that the radius of the IILR (about 1 kpc) is close to the end of the molecular bar, and the radius of the OILR (about 3 kpc) is close to the location of the twin peaks. Note that since the twin peaks are not on the major axis of the galaxy, the radii of the twin peaks from the galactic center are projected through a position angle of $\sim 30°$.[5]

If we had chosen to use the northern part instead of the southern part of the rotation curve, the location of the IILR remains at a similar radius, but the location of the OILR moves farther out in radius. This is consistent with the morphology of the central asymmetric gas distribution shown in Figure 7, where the northern gas peak at the beginning of the northern arm is farther away from the galactic center than the southern peak. These differences may result from a slightly warped galactic plane.

The identifications of the locations of the ILRs are further confirmed by the dynamical argument in § 4.2.4.

4.2.4. *Dynamical Basis for the Morphology and Kinematics of the Galaxy*

The dynamical basis for the morphology and kinematics of the central gas distribution can be understood from an analysis of orbits in an asymmetric background stellar potential. Contopoulos & Mertzanides (1977) showed that in a weakly barred potential, if the mass distribution and the pattern speed are such that two ILRs are present, then outside the OILR and inside the IILR, the dominant periodic stellar orbits are those elongated in a direction parallel to the bar potential (the so-called x_2 orbits), between the two ILRs the dominant periodic orbits are those perpendicular to the bar potential (x_1 orbits).[6] An immediate consequence is that a self-consistent bar model cannot be constructed by orbits mainly of the x_1 type, in which the orbiting mass and the gravitational potential are out of phase. Or, as the numerical models of Schwarz (1984) show, the effect of the appearance of the two ILRs is to clear an annulus between the two ILRs by sweeping the mass toward the center, which may lead to the formation of a bar inside the IILR. On the other hand, near the OILR, the crossing of the two families of periodic orbits, when combined with the pressure of the gas, leads to the crowding of the gas streamlines and thus the formation of the "twin-peaks" gas concentration near the OILR (Kenney et al. 1992; Schwarz 1984).

The spiral pattern formed near the OILR (the "twin peaks") should lead in phase with respect to the background stellar bar potential (the orientation of the large-scale stellar bar cannot be easily discerned from the optical image of this galaxy, but can nevertheless be inferred from an angular momentum argument). This allows torque exerted by the bar potential on the orbiting mass to remove angular momentum from the mass near the OILR, causing it to accrete inward. Once the inward accreting gas is swept across the space between the OILR and the IILR, it will reach the central gaseous bar structure inside the IILR. The linear offset shocks which usually form at the leading edge of the central bar can continue taking away energy and angular momentum, thus facilitating further mass accretion toward the center. The inferred orientation of the large-scale stellar bar potential, the orientation of the "twin

[4] In certain galaxies the visible spiral can extend to pass the corotation radius until the radius of the outer Lindblad resonance (OLR). But for the case of NGC 3627 it apparently could not adopt an OLR as disk boundary, since we could not identify any morphology in the inner disk that corresponds to corotation.

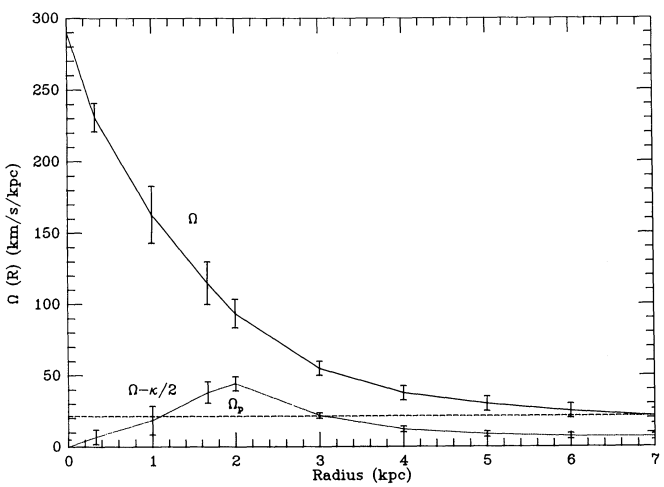

FIG. 12.—Projected angular speed, pattern speed, and the location of the inner Lindblad resonances. An uncertainty of at least 20% is expected for the value of the rotation curves.

[5] The radius of 3 kpc for OILR can be calculated as follows: At an inclination angle of 60°, the circular disk of the galaxy appears as an ellipse of axis ratio 2:1. At a 30° positron angle from the major axis of this ellipse, a radial line segment of length 2 kpc (1′) corresponds to a line segment on the major axis of length 3 kpc.

[6] In the literature the parallel family of orbits outside OILR and inside IILR had been named both as x_2 and as x_1 by different authors. So is the case for the perpendicular family of orbits between the two ILRs. The confusion in the naming scheme nonetheless did not change the characteristics of these two families of orbits. The names we used here are consistent with that used in Contopoulos & Mertzanides (1977) and with Kenney et al. (1992).

peaks," and the orientation of the central gaseous bar (which also seems to coincide with a central small stellar bar shown on the opticl image) indicate a continuous shift in phase, reminiscent of the isophote twists observed in Shaw et al. (1993).

It should be emphasized here that the presence of the ILRs, especially two widely separated ILRs which are located relatively outward in radius, is an indication that the galaxy mass distribution is very centrally condensed. This concentration includes both the stellar mass and the ISM mass. The means for the stellar mass distribution to reach higher central condensation is investigated in Zhang (1993), where it is found that it takes about 10^9 yr for mass to accrete inward for about 1 kpc, for spiral structure of the Galactic strength. This explains that, for the case of NGC 3627, 10^9 yr after interaction the high central mass concentration has just started to form, and only weak nuclear activity can be detected, which appears as a moderately strong nuclear Hα emission (Filippenko & Sargent 1985). The similar morphology and kinematics of H I and H_2 near the radius of OILR indicate that the central gaseous disk as a whole responds coherently with the instabilities in the stellar disk. Away from this radius the difference in the distributions of H I and H_2 reflects partly the difference in the interconversion of H I and H_2.

4.2.5. CO *and* H I *Spectra and the Peculiar Velocity Clump*

The spectra of CO and H I at selected positions (indicated in Figs. 3 and 5) are shown in Figures 13 and 14. The CO spectra are plotted at locations along the bar and at the twin peaks. CO emission is present at all the selected locations. A continuous rotation trend is seen through these spectra, except in spectrum F, where a second peak is also present (see discussion below). The H I spectra were plotted for locations of different clumps along the two spiral arms (A, B, C, D, E, G, H, I), the center of the galaxy (F), the eastern part of the envelope (J, K), and the peculiar noncorotating clump (L). The regular spiral arm clumps show emission at velocities which generally agree with the sense of galactic rotation. At the center of the galaxy and the outer envelope no significant emission is found. The peculiar clump L is at the highest velocity compared with the velocities of all the other spectra, and clearly does not participate in the general galactic rotation. An extended wing of emission is also seen on this spectrum. A detailed examination of spectrum G shows that there are in fact two spectral features here, and comparison with the spectra at adjacent locations show that only the high-velocity spectrum feature agrees with the trend of galactic rotation. The low-velocity feature appears to be a continuation of the peculiar motion of clump L. The double-peaked H I spectra in G can be compared with the double-peaked CO spectra in F, taken at the southern CO peak which is slightly west ($-33''$ instead of $-23''$ in relative x-coordinate) of the southern H I peak, and with a smaller synthesized beam. The difference in velocities for the low-velocity component in the CO spectrum F and H I spectrum G could be partly due to the difference in positions where the spectra were taken and partly due to the different area covered by the two beam sizes. Moreover, comparing the wide, low-velocity wing of the H I spectrum at L with the spectra at B and C, it seems plausible that clump L was a piece of the spiral arm material originally situated in between clumps B and C (where there is currently a deficiency of gas), and was pulled out of the original location and accelerated in a reverse sense during the retrograde encounter with NGC 3628. The current location of the material in clump L with respect to the disk of the galaxy cannot be decided for certain, but the fact that it still has such a high velocity and has not settled down in the galactic rotation (after the calculated 8×10^8 yr of elapsed time since the time of closest encounter) indicates that it is currently off the galactic disk and at a high latitude. It is conceivable that the cause of the stripping of this piece of material is due more to the direct

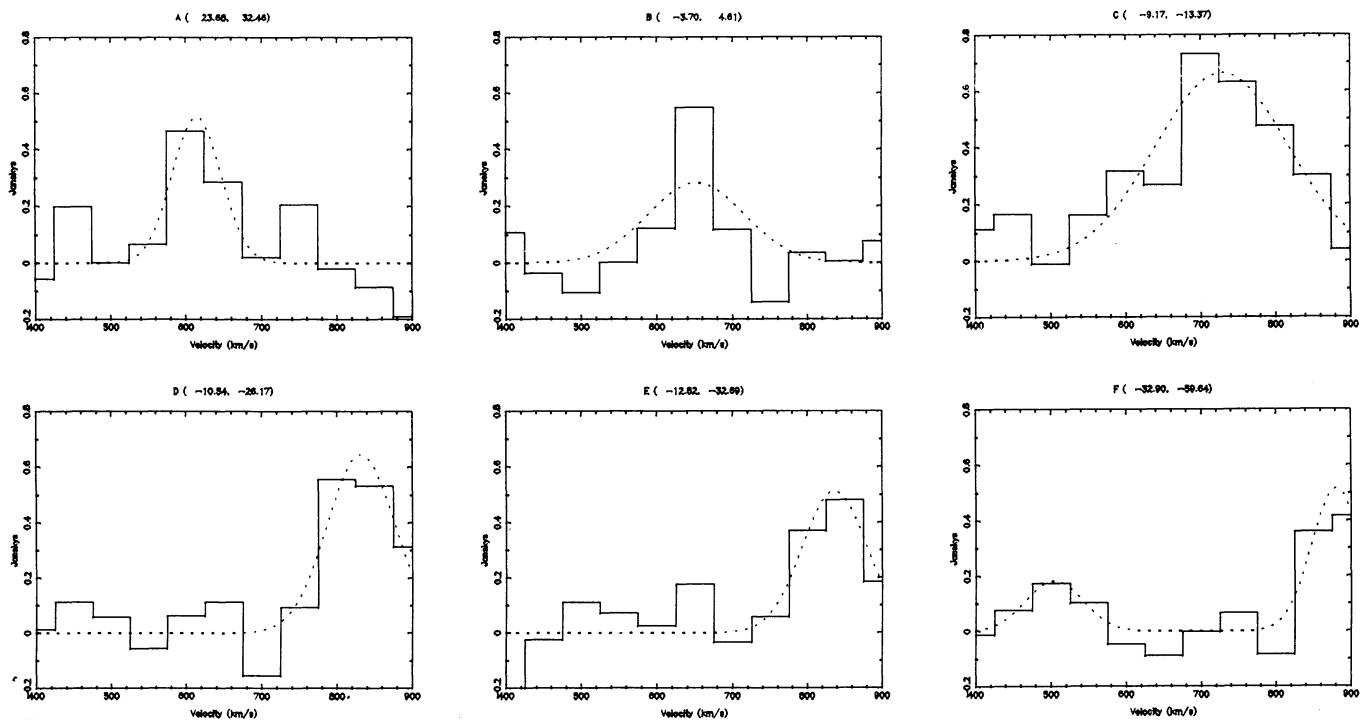

FIG. 13.—CO spectra at selected positions, together with the Gaussian fits

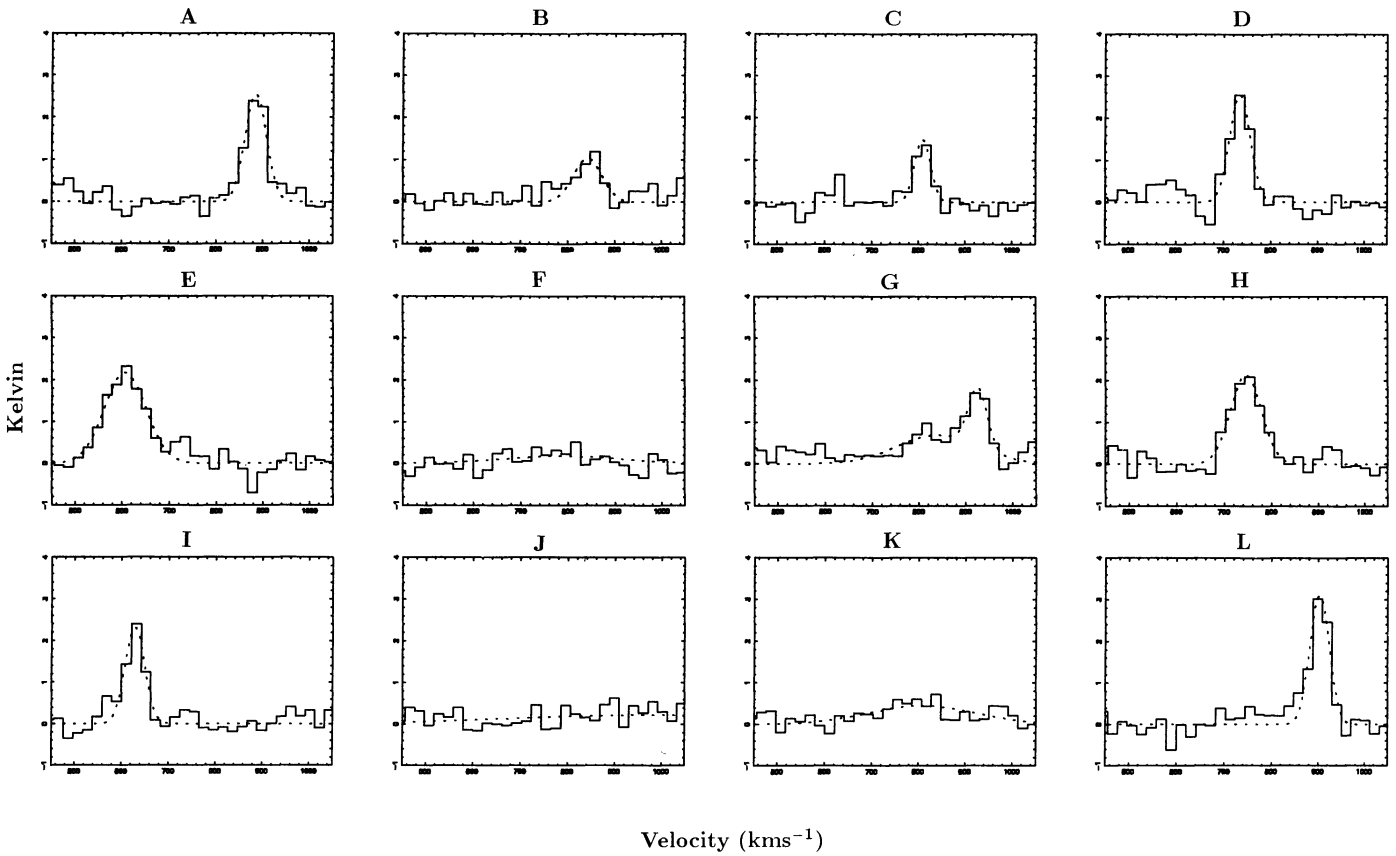

FIG. 14.—H I spectra at selected positions, together with the Gaussian fits

encounter (ram pressure) than to the gravitational force, since the closest distance between the centers of the two galaxies during the encounter is only about 25 kpc in Rots's (1978) model, which is close to the summation of the radii of NGC 3627 and NGC 3628.

4.2.6. H I *Isovelocity Contours*

Figure 15 shows the H I isovelocity contours (moment 1 map) overlaid on the H I integrated intensity map. A general galactic rotation feature is seen, modified by a few "kinks" at the location of the spiral arms, indicating the effect of the density wave on the motion of the gas. The major axis position angle used before (173°) seems to be a good fit from the isovelocity contour information. The shape of the isovelocity contours in the southern part of the map also indicates that this part of the galaxy is slightly warped, consistent with the other observed evidence that the southern part of the galaxy might be more severely distorted during the encounter.

4.3. *Implications for the General Problem of the Postinteraction Galactic Evolution*

The morphology and kinematics of the molecular and atomic gas in the central region of galaxy NGC 3627 imply certain characteristics of the postinteraction galactic evolution, which might turn out to be common for galaxies which suffered intermediate to long-range tidal disturbance, as is the case for NGC 3627. The most significant is that postineraction evolution is a well-coordinated process in the combined stellar and gaseous disk. This characteristic is demonstrated through the type of instability structures present in this galaxy: the two prominent spiral arms are the largest scale dynamic instabilities in the galactic disk, and most certainly also the first that were formed or enhanced as a result of the nonaxisymmetric gravitational perturbations to the galactic disk during the tidal encounter (Toomre 1981; Noguchi 1987; Barnes & Hernquist 1991). The large-scale spiral structure serves to transfer angular momentum outward and thus allows the central concentration of the stellar and ISM mass. The initial stage of radial mass accretion allows two inner Lindblad resonances to form and, as in the case of NGC 3627, move to larger radii as the degree of central mass concentration becomes higher. Our analysis in § 4.2 shows that these ILRs, as well as the bar structure formed inside the IILR, take over the task of removing angular momentum from the disk mass and continuing the central mass accretion process, right from the location where the spiral pattern diminishes.

The structures mapped in NGC 3627 strongly suggest that the formation of successive instabilities and the enhancement of the radial mass accretion process after galaxy interaction happen as a well-coordinated sequence of events on the combined stellar and gaseous disk, down to even the central subkiloparsec scale. It is clear that the kind of instabilities seen in the central region of NGC 3627 are not instabilities in the isolated self-gravitating gaseous disk (Shlosman et al. 1989), nor is the increase in the rate of central mass accretion caused chiefly by the increase in effective viscosity as a result of increased cloud-cloud collision (Lin et al. 1988). These are due to the following observations: (1) the central bar terminates right at the boundary of the IILR, and there is a cleared-up annulus in between the two ILRs, and (2) the gas distributions

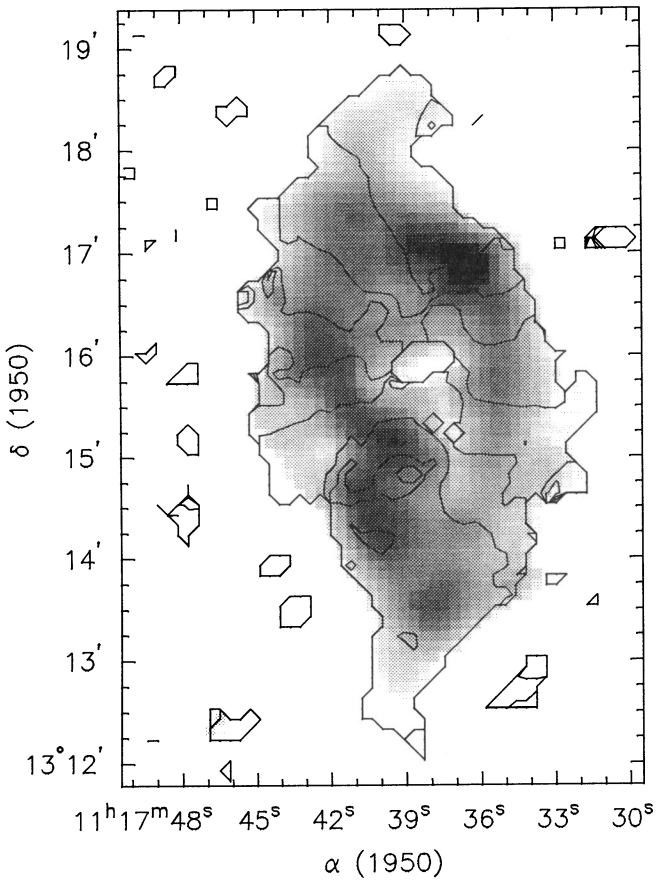

FIG. 15.—Isovelocity contours derived from H I observations, overlaid on the H I integrated intensity map shown in gray scale.

are in the form of "twin peaks" at the beginning of the spiral arms which coincide with the radius of the OILR. Neither of these morphologies can be explained by a self-gravitating viscous gaseous disk model.

Although the particular type of coherent instabilities discussed in this paper has been clearly identified so far only for galaxy NGC 3627, the formation of a bar inside the IILR under a general nonaxisymmetric galactic potential, for somewhat evolved galaxy after interaction, may be much more common than yet realized (although we do not imply here that this should be the only form of the formation of successive instabilities near the center of a galaxy). For example, in the sample of four galaxies in the Kenney et al. (1992) study, the only galaxy out of that sample which has a central molecular mass peak, which resides inside the IILR, turns out to be an interacting galaxy. The observations of Thompson (1981) showed that a larger fraction of galaxies were barred in the core of the Coma Cluster than outside, which suggests a possible correlation between galaxy interaction and the formation of bars in the center of a galaxy. Numerical simulations by Byrd et al. (1986) on the effect of the interactions on the subsequent galactic evolution indicate that a bar usually forms in a model galaxy under strong perturbations. The bar-forming phenomena in the perturbed disks are also observed in the numerical models of Noguchi (1987). It should be emphasized, however, that oftentimes the tidal torque during a galactic encounter does not influence the mass distribution of the central region of the disk directly and immediately, but instead is mediated by the disk spiral density wave, which is excited or amplified by the tidal torque of the encounter. This is true especially for high-speed encounters. This shows up in the numerical simulations of Byrd & Howard (1990) and Hernquist (1990). The dynamical basis for the coevolution of the stellar and gaseous mass distribution in a galactic disk which possesses a prominent spiral structure is discussed in Zhang (1992, 1993).

Certainly, more high-resolution maps of the inner region of postinteraction galaxies (or galaxies which have companions) are needed in order to clarify the different types of instability structures in the inner galaxy. If it turns out that the ILR-assisted mass accretion in the inner galactic disk is common among postinteraction galaxies, this would imply that the evolution of the stellar disk plays an important role in the evolution of the galactic gas distribution, and in the evolution of normal to active galaxies.

5. CONCLUSIONS

The high-resolution CO and H I observations of NGC 3627 demonstrate that the effects of its past encounter with NGC 3628 show up in the following forms:

1. The extremely high central mass concentration, indicated by the steep-rising rotation curve near the center and by the presence of the two outward-located ILRs. The central concentration of gas mass inside the IILR is in the form of a molecular bar. The location of the OILR coincides with the "twin peaks" of gas distribution at the beginning of the spiral arms, where gas streamline crowding caused the accumulation of gas mass.
2. The high ratio of molecular to atomic mass, possibly caused by the combined effect of the capture of the H I outer envelope by NGC 3628 during the encounter, and by an enhanced conversion rate of the atomic to molecular mass in the central region of the galaxy, due to enhanced shock activities.
3. A resolved noncorotating clump of H I material, which appears to have been removed from one of the spiral arms, possibly due to the ram pressure of the direct contact during the close encounter. The effect of interaction also shows up through the extremely prominent spiral arm and dust lane structures shown on the optical image (Arp 1966).

The current work supports the thesis that tidal encounters among galaxies can lead to the formation of successive gravitational instabilities in the galactic disk and the triggering of nuclear activity. The tidal interaction can also trigger efficient conversion of atomic to molecular gas to fuel a starburst. The new element that the current result adds to the general postinteraction evolution scenario is the coordinated formation of successive instabilities in the combined stellar and gaseous disk after galaxy interaction. The prominent spiral structure formed after galaxy interaction leads to rapid radial accretion of disk mass, and this in turn leads to the formation of ILRs. Once formed, the ILRs continue the task of removing angular momentum from the disk mass, which was carried out by the spiral structure in the outer disk, and are able to channel the gas down to the central subkiloparsec region to fuel nuclear activity.

We thank the staff at the Hat Creek Observatory and at the VLA for their assistance during observations. This research was partially supported by NSF grant AST 91-00307.

REFERENCES

Adams, T. F. 1977, ApJS, 33, 19
Appleton, P. N., & Hughes, D. H. 1988, in Dust in the Universe, ed. M. E. Bailey & D. A. Williams (Cambridge: Cambridge Univ. Press)
Arp, H. C. 1966, Atlas of Peculiar Galaxies (Pasadena: CIT Press)
Barnes, J. E., & Hernquist, L. 1991, ApJ, 370, L65
———. 1992, ARA&A, 30, 705
Byrd, G. G., & Howard, S. 1990, in Dynamics and Interactions of Galaxies, ed. R. Wielen (Heidelberg: Springer-Verlag)
Byrd, G. G., Valtonen, M. J., Sundelius, B., & Valtaoja, L. 1986, A&A, 166, 75
Contopoulos, G., & Mertzanides, C. 1977, A&A, 61, 477
Dahari, O. 1985, ApJS, 57, 643
de Vaucouleurs, G. 1975, in Stars and Stellar Systems, Vol. 9, Galaxies and the Universe, ed. A. Sandage, M. Sandage, & K. Kristian (Chicago: Univ. Chicago Press), 309
de Vaucouleurs, G., de Vaucouleurs, A., & Corwin, H. G. 1976, Second Reference Catalogue of Bright Galaxies (Austin: Univ. Texas Press) (RC2)
Dressel, L. L., & Condon, J. J. 1976, ApJS, 31, 187
Efstathiou, G. P. E. 1990, in Dynamics and Interactions of Galaxies, ed. R. Wielen (Heidelberg: Springer-Verlag), 2
Filippenko, A. V., & Sargent, W. L. W. 1985, ApJS, 57, 503
Haynes, M. P., Giovanelli, R., & Morton, S. R. 1979, ApJ, 229, 83
Hernquist, L. 1990, in Dynamics and Interactions of Galaxies, ed. R. Wielen (Heidelberg: Springer-Verlag)
Hutchings, J. B., & Campbell, B. 1983, Nature, 303, 584
Kenney, J. D. P., Wilson, C. D., Scoville, N. Z., Devereux, N. A., & Young, J. S. 1992, ApJ, 395, L79
Kormendy, J., & Bahcall, J. N. 1974, AJ, 79, 671
Lin, D. N. C., Pringle, J. E., & Rees, M. J. 1988, ApJ, 328, 103
Noguchi, M. 1987, MNRAS, 228, 635
Roberts, W. W., Huntley, J. M., & van Albada, G. D. 1979, ApJ, 233, 67
Rohlfs, K. 1977, Lectures on Density Wave Theory (Heidelberg: Springer-Verlag), 95
Rots, A. H. 1978, AJ, 83, 219
Schwarz, M. P. 1984, MNRAS, 209, 93
Scoville, N. Z., & Young, J. S. 1983, ApJ, 265, 148
Shaw, M. A., Combes, F., Axon, D. J., & Wright, G. S. 1993, A&A, 273, 31
Shlosman, I., Frank, J., & Begelman, M. C. 1989, Nature, 338, 45
Simkin, S. M., Su, H. J., & Schwarz, M. P. 1980, ApJ, 237, 404
Stockton, A. 1982, ApJ, 257, 33
Sulentic, J. W., Keel, W. C., & Telesco, C. M., ed. 1990, in IAU Colloq. 124, Paired and Interacting Galaxies, ed. J. Sulentic & W. Keel (NASA Publ. 3098)
Thompson, L. A. 1981, ApJ, 178, 623
Toomre, A. 1978, in IAU Symp. 77, Structure and Properties of Nearby Galaxies, ed. E. M. Berkhuijsen & R. Wielebinski (Dordrecht: Reidel), Review Lecture
Toomre, A. 1981, The Structure and Evolution of Normal Galaxies, ed. S. M. Fall & D. Lynden-Bell (Cambridge: Cambridge Univ. Press), 111
Toomre, A., & Toomre, J. 1972, ApJ, 178, 623
Ulich, B. L. 1981, AJ, 86, 1619
Warner, P. J., Wright, M. C. H., & Baldwin, J. E. 1973, MNRAS, 163, 163
Wielen, R., ed. 1990, Dynamics and Interactions of Galaxies (Heidelberg: Springer-Verlag)
Young, J. S., & Scoville, N. Z. 1982a, ApJ, 258, 467
———. 1982b, ApJ, 260, L11
Young, J. S., Tacconi, L. J., & Scoville, N. Z. 1983, ApJ, 269, 136
Zepf, S. E., & Koo, D. C. 1989, ApJ, 337, 34
Zhang, X. 1992, Ph.D. thesis, Univ. California, Berkeley
———. 1993, in preparation
Zwicky, F. 1956, Erg. exakt. Naturwiss., 29, 344